2007

Fibre Bragg Grating Sensors for Acoustic Emission and Transmission Detection Applied to Robotic NDE in Structural Health Monitoring

Graham Wild
Edith Cowan University

Steven Hinckley
Edith Cowan University

10.1109/SAS.2007.374388

SAS 2007 – IEEE Sensors Applications Symposium
San Diego, California USA, 6-8 February 2007

Fiber Bragg Grating Sensors for Acoustic Emission and Transmission Detection Applied to Robotic NDE in Structural Health Monitoring

Graham Wild, *Student Member, IEEE,* Steven Hinckley, *Member, IEEE*
School of Engineering and Mathematics
Edith Cowan University,
100 Joondalup Drive,
Joondalup, WA, Australia, 6027

***Abstract*—Distributed acoustic emission sensors are used in Structural Health Monitoring (SHM) for the detection of impacts and/or strain, in real time. Secondary damage may result from the initial impact or strain. This damage may include surface pitting, erosion, or cracking. This type of damage may not be detectable by the SHM system, specifically in passive fiber optic based sensing systems. The integration of Non-Destructive Evaluation (NDE) by robots into SHM enables the detection and monitoring of a wider variety of damage. Communicating via acoustic transmissions represents a wireless communications method for use by NDE inspection robots to communicate with an integrated SHM system that does not require any additional hardware, as piezoelectric transducers are commonly used in the NDE of materials.**

In this paper, we demonstrate the detection of both acoustic emissions and transmissions with a Fiber Bragg Grating (FBG) sensor. The acoustic communications channel comprises of a piezoelectric transmitter, an aluminum panel as the transmission medium, and a FBG receiver. Phase Shift Keying was used to encode the acoustic transmissions. Results for the frequency and transient response of the channel are presented.

***Index Terms*—Wireless and Networked Sensors; Integrated System Health Management (ISHM); Nondestructive Evaluation and Remote Sensing**

I. Introduction

THE use of Acoustic Emission (AE) sensors in aerospace vehicle Structural Health Monitoring (SHM) has been established in the literature [1], [2]. Distributed AE sensors can be used for the real time detection and monitoring of impacts and strain. However, secondary damage can result from the initial impact or strain. Secondary damage can include surface pitting, erosion, and cracking. This represents a challenge to a SHM system based only on AE detection, as these types of damage cannot be monitored by passive AE sensing. Active devices can be incorporated and used to interrogate the structure; however, this requires a more complex system incorporating pattern recognition, or other advanced signal processing tools, to detect the presence of secondary damage. Secondary damage monitoring also represents a challenge for photonic based sensing systems, due to the fact that the majority of photonic sensors are passive, i.e. they cannot be used as actuators. There are also other types of damage that cannot be monitored using AEs, such as corrosion.

In advanced Non-Destructive Evaluation (NDE) systems, robots have been proposed to carry out autonomous inspection in aerospace vehicles [3]. Robotic based NDE represents a method of overcoming the challenges of monitoring secondary damage in SHM systems. Robotic agents can be used to interrogate the structure together with the embedded sensors, enabling the integrated system to detect and monitor a wider range of measurands. Even if the structure has embedded sensors for detecting damage, e.g. chemical sensors for corrosion detection, the use of an autonomous inspection robot will allow for a more detailed inspection of the damage, beyond the capability of the SHM system.

In smart materials and structures, where sensors are interfaced with embedded distributed electronics, the information from the sensors needs to be moved from the point of detection to the central processor or human interface. Both wire [4] and wireless RF [5] systems have been proposed. Communicating via acoustic transmissions [6] represents wireless communications methods for use by autonomous robots in the SHM of aerospace vehicles with embedded distributed intelligence and sensing systems. An acoustic communications channel does not require the addition of any hardware, as piezoelectric transducers are commonly used in the NDE of materials. The implementation of acoustic communications only requires the addition of relevant software.

II. Theory

A. Acoustic Emissions

AEs are stress waves that propagate through a material, which can be generated internally by microcracks or inclusion de-cohesion under external loading [6]. Rapid local stress redistribution as a result of loading causes the material defects

to release elastic energy. The energy results from crack growth, crack surface movement, or dislocations. AEs can also be generated by phase transformation or melting. These internal sources of AEs represent a passive as well as a static method of damage detection. AE can also be generated by external sources, specifically impacts, and actively generated by actuators, such as piezoelectric transducers.

B. *Fiber Bragg Grating Acoustic Emission Sensor*

A Fiber Bragg Gratings (FBG) is a spectrally reflective component that uses the principle of Bragg reflection. The grating is made up of alternating regions of high and low refractive indices. The periodic grating acts as a filter, reflecting a narrow wavelength range, centered about a peak wavelength. This wavelength is known as the Bragg wavelength, λ_B, and is given by,

$$\lambda_B = 2n\Lambda, \tag{1}$$

where n is the average refractive index of the grating, and Λ is the grating period. Any measurand that has the ability to affect either the refractive index or the grating period can be measured using an FBG as a sensor. Sensitivity specifically applies to the grating period which is effectively a length measurement. Hence, any quantity that varies a length, e.g. temperature, pressure or strain, can be measured. Therefore the change in the measurand corresponds to a change in the reflected wavelength. The relative change in the Bragg wavelength can be approximated as,

$$\frac{\Delta\lambda_B}{\lambda_B} = C_S S + C_T \Delta T \tag{2}$$

where C_S is the coefficient of strain, S, C_T is the coefficient of temperature, and ΔT is the change in temperature.

Methods for using FBGs as AE sensors have been outlined in a number of references [8], [9], and [10]. In these FBG AE sensors, the strain induced shift in the wavelength is converted into an intensity change. This is achieved by simply choosing the appropriate optical bias point. In Figure 1, showing the reflectivity as a function of wavelength, there is an almost linear region, centered about λ_0. This linearity occurs between reflectivities of 20 to 80 percent. Using this region, a linear intensity based optical fiber AE sensor can be realized. This requires the use of a narrow linewidth laser source operating about λ_0, and a photodetector to detect the reflected laser light.

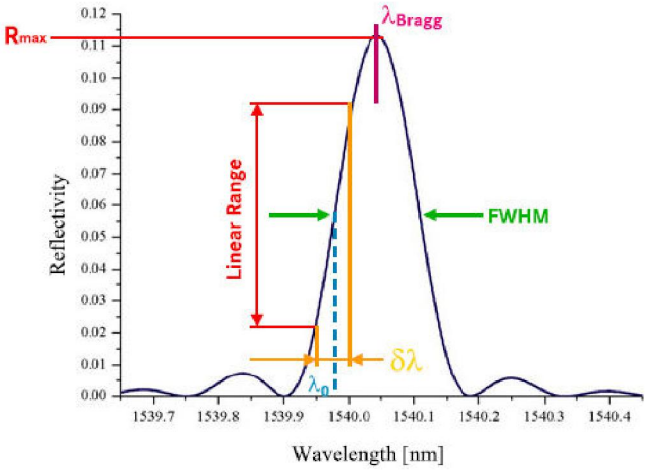

Fig. 1. The relevant parameters for a FBG AE sensor, shown on a reflectivity plot [10].

C. *Communications Theory*

The digital communications method chosen for the acoustic transmissions was phase shift keying (PSK), specifically binary phase shift keying (BPSK). In PSK, the digital information is encoded onto the carrier wave via a phase modulation. The state of each bit of information is determined according to the state of the preceding bit. If the phase of the carrier wave does not change, then the logic level stays the same. If the phase of the carrier wave changes by 180 degrees, then the logic level changes, from zero to one, or from one to zero.

Decoding the received PSK signals is performed by using some simple mathematics to retrieve the phase information. For an ideal carrier wave of frequency f_c, a PSK signal can be described as,

$$f(t) = A_0 \cos\left(2\pi f_c t + \phi(t)\right). \tag{3}$$

If the receiver knows f_c, the phase of the received signal can be determined. This is achieved by multiplying the signal, (3), by a synchronous sine and cosine. This gives,

$$\begin{aligned} g(t) &= A_0 \cos(2\pi f_c t + \phi(t)) \times \sin(2\pi f_c t) \\ &= \frac{A_0}{2}[\sin\left(4\pi f_c t + \phi(t)\right) + \sin\left(\phi(t)\right)], \end{aligned} \tag{4}$$

and,

$$\begin{aligned} h(t) &= A_0 \cos(2\pi f_c t + \phi(t)) \times \cos(2\pi f_c t) \\ &= \frac{A_0}{2}[\cos\left(4\pi f_c t + \phi(t)\right) + \cos\left(\phi(t)\right)]. \end{aligned} \tag{5}$$

These two components are called the in-phase (I) and quadrature (Q) components. This results in the generation of high and low frequency components of I and Q, where the low frequency component is the sine or cosine of the time dependent phase. Using a low pass filter, high frequency components are removed leaving only the phase components,

$$g(t) = \frac{A_0}{2}\sin\left(\phi(t)\right), \tag{6}$$

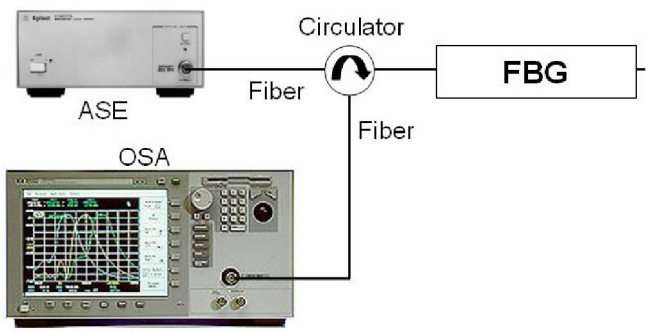

Fig. 2. Optical circuit used to characterize FBG and determine the operating point of the sensor.

and,

$$h(t) = \frac{A_0}{2}\cos(\phi(t)). \tag{7}$$

Then by taking the arctan of I on Q, the time dependent phase information is recovered,

$$\begin{aligned} y(t) &= \arctan\left(\frac{g(t)}{h(t)}\right) \\ &= \arctan\left(\frac{\sin(\phi(t))}{\cos(\phi(t))}\right) \\ &= \arctan(\tan(\phi(t))) \\ &= \phi(t). \end{aligned} \tag{8}$$

The filter used was a raised cosine filter [11]. The decoding algorithm and the filtering were implemented in Matlab™ [12].

III. Experiments

A. Determining the FBGs Operating Point

The experimental setup for determining the operating point of the FBG sensor is show in Figure 2. A broadband Amplified Spontaneous Emission (ASE) light source was used as the input to the FBG. The Optical Spectrum Analyzer (OSA) was then used to measure the relevant wavelengths. The output of the tunable laser source was also measured using the OSA. Note the use of a circulator rather than the conventional coupler. The circulator was used to ensure isolation between the relevant optical paths.

B. Experimental Setup for Acoustic Transmissions

The experimental setup used for the acoustic transmissions is shown in Figure 3. The setup consists of several layers;

- a PZT (lead zirconate titanate) transducer as the transmitter (2.1 millimeters thick, 10 millimeters radius),
- a coupling medium,
- the material to be communicated through, specifically an aluminum panel (1.5 millimeters thick), and
- the FBG receiver.

The FBG receiver includes a tunable laser, circulator, and photodetector. Two coupling methods were used for the FBG. One FBG was bonded to an aluminum panel; the second was coupled to the aluminum panel with acoustic coupling gel. An amplifier was not used on the input to the PZT transmitter or the output from the photodetector, nor was an optical amplifier used.

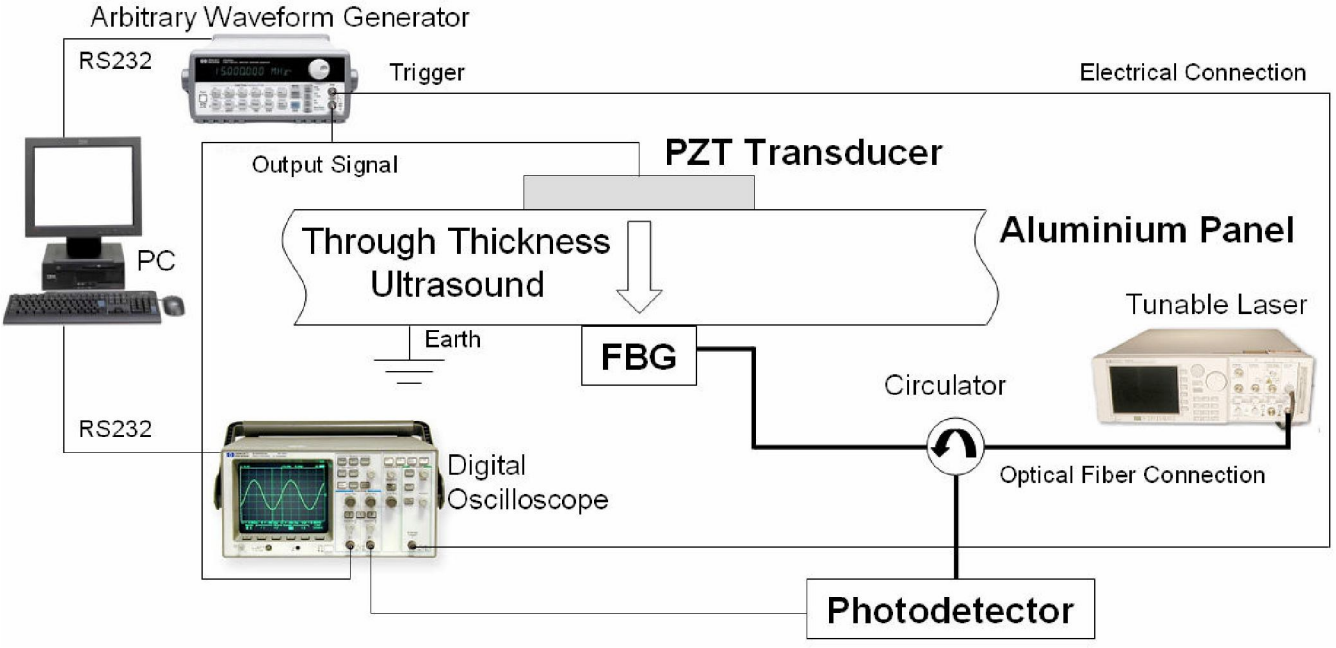

Fig. 3. The setup for the acoustic transmission experiments. The same optical circuit is used in the AE detection

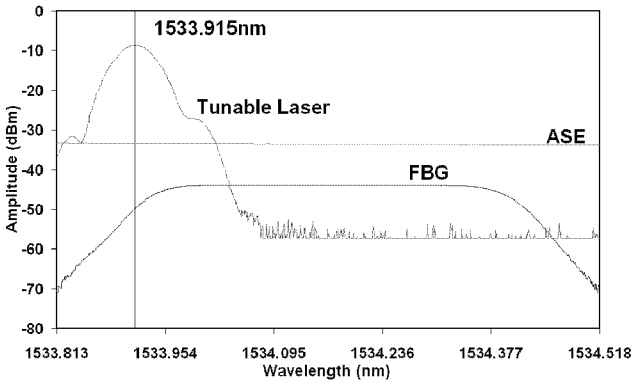

Fig. 4. The spectral response of the FBG, ASE, and the tunable laser, centered at the operating wavelength of 1533.915nm.

C. *Acoustic Emissions*

AEs were generated to determine if the FBG could be used for their detection. AEs were generated via a pencil lead break test, located 100 millimeters away from, and along the optical axis of, the FBG. AEs were also generated by drop tests, using a nut (0.7 grams) and a bolt (3.7 grams), the specimens were dropped from a height of 300 millimeters, directly over the FBG. For the acoustic emissions tests, the PZT transmitter and the function generator shown in Figure 3 were not required.

D. *Acoustic Transmissions*

The frequency response of the acoustic transmission channel was measured using a continuous sine wave at maximum voltage, 10 Volts peak. The frequency was then varied from 100 kilohertz to 2 megahertz recording the received amplitude at every kilohertz.

The transient response of the acoustic transmissions channel was measured using a sine wave burst, again at maximum voltage. The burst count was increase from 1 to the number required for maximum amplitude to be reached, hence, representing the onset of steady state.

The results from the frequency response were used to determine the carrier wave frequency for the acoustic transmissions. The communications signals were generating in Agilent's Waveform Editor software for the 33120A arbitrary waveform generator. The signals were then flashed to the device via the computer interface. Waveforms using a square wave carrier were generated with data rates at 1/400, 1/200, 1/100, and 1/50 times the carrier wave frequency.

IV. Results

All of the results presented use the FBG coupled to the aluminum panel with acoustic coupling gel.

A. *Operating point*

Figure 4 shows the spectral response of the OSA, FBG, and tunable laser set to the operating point. The location of the peak corresponds to a value below the linear region of the FBGs spectral response, this is due to the linewidth of the tunable laser being too broad, and hence, a lower value had to be used.

B. *Channel Response*

The frequency response of the FBG is shown in Figure 5. Since bit rate is related to the bandwidth, using the broadest peak would, in theory, give the highest bit rate for transmissions. Although the broadest peak is clearly located at 1008.1 kilohertz, the 630.6 kilohertz peak was selected due to the improved signal to noise ratio, which is significant for communications signals.

The transient response at 630 kilohertz is show in Figure 6. The transient response time was 240 microseconds, corresponding to 150 cycles.

C. *Acoustic Emissions*

The results of the drop tests are shown in Figure 7, and the pencil break test result is show in Figure 8. The drop tests results are shown on a 1 millisecond per division scale, and the lead pencil break test is show on a 100 microsecond per division scale. The voltage scales vary between all the images.

D. *Acoustic Transmissions*

As a result of the frequency response, communications signals were generated using a carrier wave frequency of 630 kilohertz. The decoded acoustic communications signals are shown in Figure 9. The first three signals successfully decoded with no bit errors. The final signal did not decode successfully.

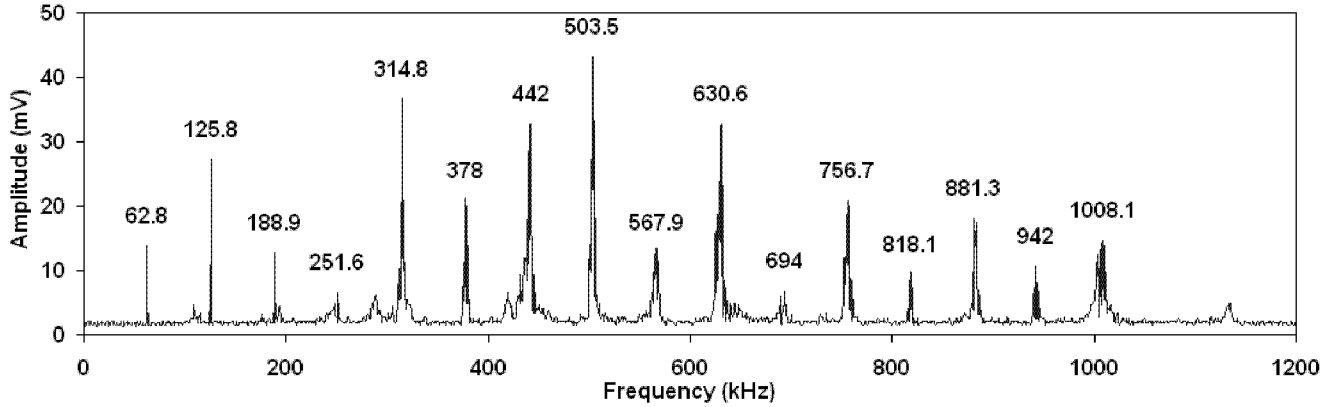

Fig. 5. The frequency response of the communications channel, PZT–Al–FBG. The peaks (with frequencies above) occur with a separation of around 63 kHz. Note, no signals were detected above 1.2MHz

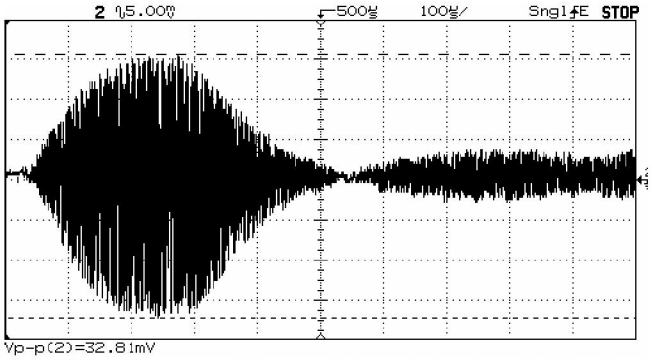

Fig. 6. Transient response of the acoustic transmission channel, 150 cycles at 630kHz.

V. Discussion

The first observation of note was the fact that while all experiments were performed using both a FBG coupled to the aluminum, and a FBG bonded to the panel, results were only obtained for the coupled FBG. The explanation for this may have previously been suggested by Lee and Tsuda [13], who reported the improved performance of FBG acoustic sensors, by using strain isolated FBG temperature sensors. The bonded FBG is encased in epoxy, which may make it less sensitive to the small dynamic strain induced by the acoustic emissions and transmissions. Future work is to be performed to confirm this hypothesis.

The frequency response of the communications channel may present a problem if it represents the frequency response of the FBG alone. This requires the use of different piezoelectric transducers, specifically a broadband transducer to test the response of the FBG alone.

The response of the FBG to the impact tests was promising. There is a significant increase in signal amplitude from 20 millivolts in the bottom plot of Figure 7, to the 40 millivolts in the top plot of Figure 7. This increase in received amplitude corresponds to the increase in mass from the nut to the bolt. The change in frequencies generated is also significant. This is related to the impact interaction, as the nut was dropped so it landed on its large flat surface, while the bolt landed on a point. The sounds generated were audibly different. The bolt generated a distinct signal which would correspond to the frequency of approximately 3 kilohertz shown in the plot. The sound generated by the nut was hard to characterize, the signal is noisy, as more frequencies were generated. Future work will look at signal processing methods for feature extraction to characterize impacts.

The FBG was also sensitive enough to detect the AE from the lead pencil break test. The signal is comprised of two main frequencies. The low frequency component, which would correspond to the audible crack of the pencil lead, is about 5 to 6 kilohertz. The high frequency component is more interesting. The frequency is approximately 63 kilohertz, which is the first resonant frequency show in the frequency response, Figure 5. If Figure 5 is the frequency response of the FBG sensors, then the sensor may intrinsically possess the

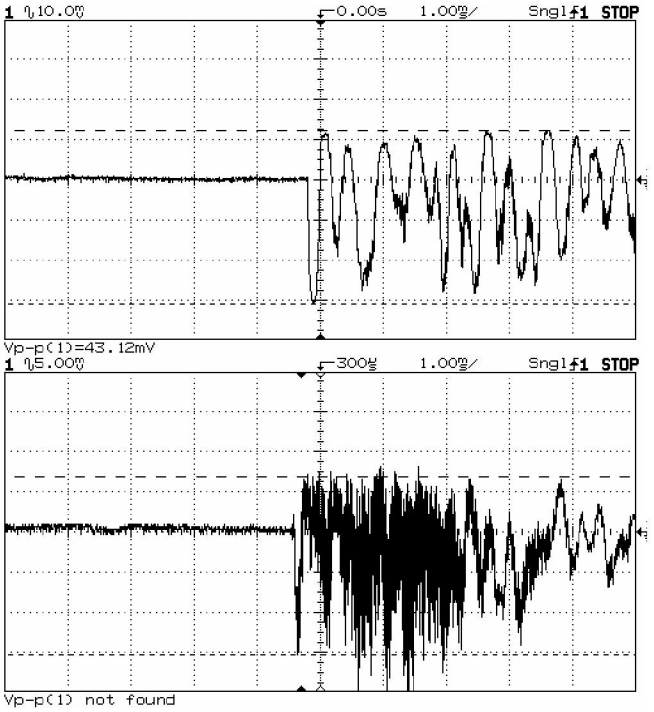

Fig. 7. Results for the drop test using the bolt (top), using the nut (bottom).

ability to decompose the signal into the resonant frequency 'channels', enabling simple analog processing of the signal. The signal could be filtered into its frequency components, and the amplitudes of the individual frequency components could be the features to be extracted and compared.

The achievable data rate for the acoustic transmissions, 6.3 kilobits per second for a carrier frequency of 630 kilohertz, was lower than expected. The low bit rate is related to the long transient response time of the FBG receiver. This then leads to the question of why the transient response of the FBG sensor is so long. One limitation that needs to be addressed is the small dimension of the aluminum panel used. The small area may introduce edge reflections that interfere with the generated signal. This will be addressed in future work to determine additional information about the transient response, and how it may be reduced. Suggestions include trying to embed the fiber in soft set epoxy resin or silicone rubber to dampen its vibration, while trying to maintain the response to the small dynamic strain.

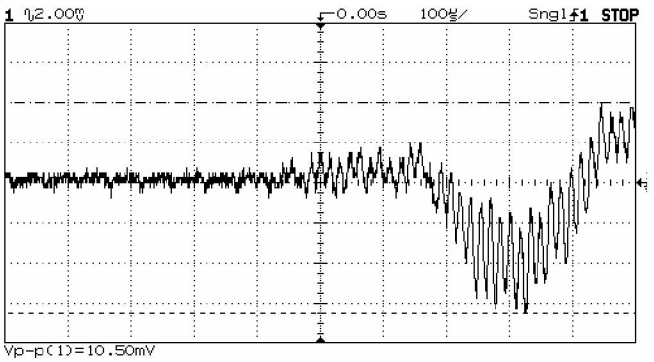

Fig. 8. Results for the pencil lead break test.

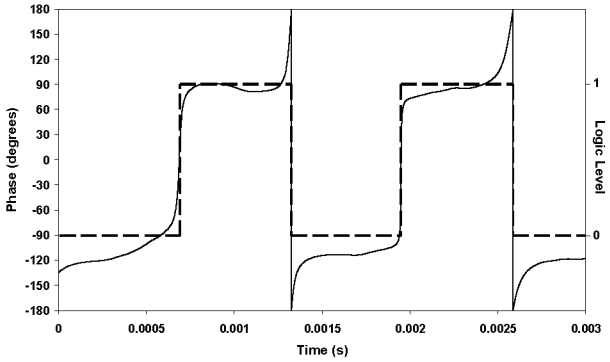

a)

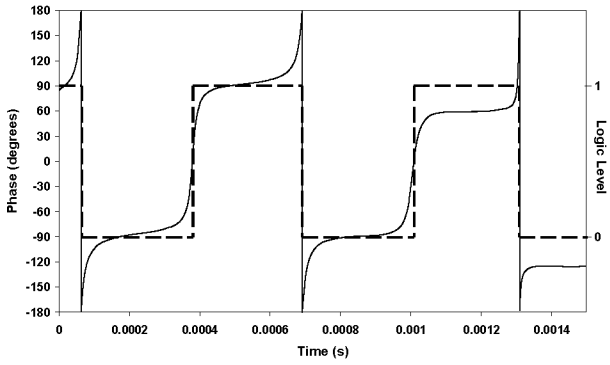

b)

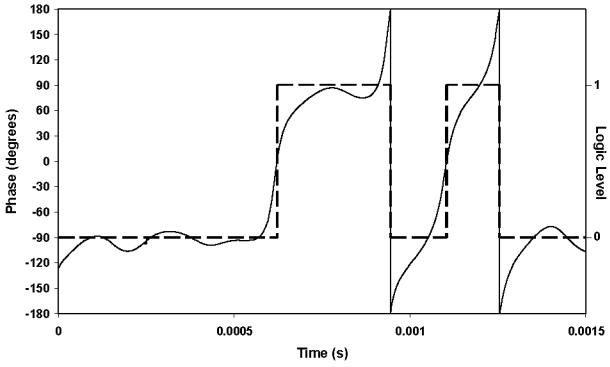

c)

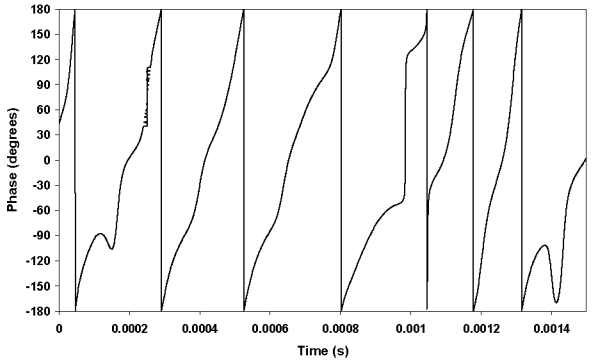

d)

Fig. 9. Decoded acoustic transmission signals (solid lines) showing the recovered information (dashed lines). With carrier wave frequencies and data rates of a) 635.68kHz and 1.5892kbps, b) 635.68kHz and 3.1784kbps, c) 635.68kHz and 6.3568kbps and d) 635.68kHz and 12.7136kbps with a bit error rate of 0.159.

VI. Conclusion

A FBG sensor has been used for the successful detection of acoustic emissions and transmissions. The FBG sensor has sufficient sensitivity to detect the AE from a pencil break test. Also, the ability of the sensor to detect AEs from drop tests was demonstrated. The FBG AE sensor, that is to be used in a distributed SHM sensor network, was then used for the detection of acoustic transmissions. Successful communication was achieved via the acoustic transmissions. Using PSK and a carrier frequency of 630 kilohertz, a data rate of 6.3 kilobits per second was demonstrated, and the phase diagram suggests that up to 10 kilobits per second could be achievable. The data rate is sufficient for the transfer of information such as coordinates and thickness measurements from an NDE robot to the distributed SHM system. Higher data rates, to transfer more information, and possibly images, may be achievable using higher carrier frequencies. This and the use of other digital encoding methods will be the focus of future work on acoustic communications.

References

[1] C. Marantidis, C. B. Van Way, and J. N. Kudva, "Acoustic-emission sensing in an on-board smart structural health monitoring system for military aircraft," in Smart Structures and Materials 1994: Smart Sensing, Processing, and Instrumentation, Proc SPIE, Vol. 2191, pp. 258-264, 1994.

[2] D. C. Price et al, "An Integrated Health Monitoring System for an Ageless Aerospace Vehicle," in Structural Health Monitoring 2003: From Diagnostics & Prognostics to Structural Health Management, Fu-Kuo Chang, ed., DEStech Publications, Lancaster PA, pp. 310-8, 2003.

[3] B. Bahr, "Automated Inspection for Aging Aircraft," in International Workshop on Inspection and Evaluation of Aging Aircraft, pp. 18-21, 1992.

[4] M. Hedley, M. Johnson, C. Lewis, D. Carpenter, H. Lovatt, D. Price, "Smart Sensor Network for Space Vehicle Monitoring," in Proceedings of the International Signal Processing Conference, Dallas Tx, March 2003.

[5] B. F. Spencer, M. E. Ruiz-Sandoval, N. Kurata, "Smart Sensing Tchnology: Opportunities and Challenges," Structural Control and Health Monitoring, Vol. 11, pp. 349-368, 2004.

[6] G. Wild, "Design and Evaluation of an Electro-Acoustic Communications Channel for use by Autonomous Agents in the Structural Health Monitoring of Ageless Aerospace Vehicles," Honours Thesis, Edith Cowan University, 2005.

[7] W. Staszewski, C. Boller, G. Tomlison, Health Monitoring of Aerospace Structures: Smart Sensor Technologies and Signal Processing, Wiley, West Sussex, 2004.

[8] P. A. Fomitchov, S. Krishnaswamy, "Fiber Bragg Grating Ultrasound Sensor for Process Monitoring and NDE Applications," Review of Quantitative Nondestructive Evaluation, Vol. 21, pp. 937-944, 2002.

[9] P. A. Fomitchov, S. Krishnaswamy, "Response of a Fiber Bragg Grating Ultrasonic Sensor," Optical Engineering, Vol. 42, pp. 956-963, 2003.

[10] D. C. Betz, G. Thursby, B. Culshaw, W. J. Staszewski, "Acousto-Ultrasonic Sensing using Fiber Bragg Gratings," Smart Materials and Structures, Vol. 12, pp. 122-128, 2003.

[11] J. Proakis, M. Salehi, Communication Systems Engineering, Prentice Hall, New Jersey, 1994.

[12] Mathworks Inc.

[13] J. R. Lee, H. Tsuda, "Acousto-ultrasonic sensing using capsular fibre Bragg gratings for temperature compensation," Measurement Science and Technology, Vol. 17, No. 11, pp. 2920-2926, 2006.